ARTICLE

# Thermionic Field Emission Transport in Carbon Nanotube Transistors

David J. Perello,[†] Seong Chu Lim,[‡] Seung Jin Chae,[‡] Innam Lee,[†] Moon. J. Kim,[§] Young Hee Lee,[‡,*] and Minhee Yun[†,*]

[†]Department of Electrical Engineering, University of Pittsburgh, Pittsburgh Pennsylvania 15219, United States, [‡]Department of Physics, Department of Energy Science, Sungkyunkwan Advanced Institute of Nanotechnology, Suwon 440-746, Republic of Korea, and [§]Department of Materials Science and Engineering, University of Texas — Dallas, Richardson, Texas 75080, United States

**ABSTRACT** With experimental and analytical analysis, we demonstrate a relationship between the metal contact work function and the electrical transport properties saturation current ($I_{sat}$) and differential conductance ($\sigma_{sd} = \partial I_{sd}/\partial V_{sd}$) in ambient exposed carbon nanotubes (CNT). A single chemical vapor deposition (CVD) grown 6 mm long semiconducting single-walled CNT is electrically contacted with a statistically significant number of Hf, Cr, Ti, Pd, and Au electrodes, respectively. The observed exponentially increasing relationship of $I_{sat}$ and $\sigma_{sd}$ with metal contact work function is explained by a theoretical model derived from thermionic field emission. Statistical analysis and spread of the data suggest that the conduction variability in same CNT devices results from differences in local surface potential of the metal contact. Based on the theoretical model and methodology, an improved CNT-based gas sensing device layout is suggested. A method to experimentally determine gas-induced work function changes in metals is also examined.

**KEYWORDS:** carbon nanotube · thermionic field emission · schottky barrier · electrical transport · saturation current · differential conductance

Current modulation in carbon nanotube field effect transistors (CNTFETs) is dominated by field-adjusted energy barriers at the contacts,[1−5] in contrast to Si-based devices.[6] Without chemical treatment, the metal-contact work function determines the CNT device polarity,[7,8] applicable in advanced adaptive logic circuits[9] and dopant-free complementary metal-oxide semiconductor (CMOS) circuitry.[10−12] However, previous attempts at understanding the contact physics of CNTFETs[13−16] are complicated by the usage of CNT with varying diameter and the lack of an analytical CNT transport model. Therefore, here we report systematic experimental and theoretical analysis relating metal-contact work function and electrical transport properties saturation current ($I_{sat}$) and differential conductance ($\sigma_{sd}$) in CNTFETs, incorporating a theoretical model analytically derived from thermionic field emission. Previous limitations are overcome with measurement, statistical analysis, and data fitting from ∼100 Hf, Cr, Ti, Au, and Pd contacts on a single CNT. Further analysis suggests the model is applicable for quantitative nanotube-based gas sensing and for noninvasive metal work-function measurement.

## RESULTS

CNTFETs are fabricated using e-beam lithography and physical evaporation onto centimeter long, aligned, laminar flow grown thermal chemical vapor deposition (CVD) CNTs.[17] Metal contacts were placed in a linear fashion along the tube length with an equidistance of 1 $\mu$m gap (Figure 1a). After fabrication, additional CNTs on the sample were removed with 100−150 W $O_2$ plasma, while areas containing FETs were covered with protective sacrificial layer of photo resist. This resist was removed, and the sample was cleaned twice by UV exposure and further rinsed in acetone to remove any residue. Atomic force microscopy (AFM) measurements confirmed the cleanliness of the sample. We focus on two samples in this report, the first contains 120 electrodes (114 devices) on a single 6 mm long semiconducting CNT of 1.7 nm diameter with 86 devices electrically active at the first measurement (75.4% yield). The diameter was confirmed by AFM, and the lack of 100% yield results from regions where the single CNT was damaged during fabrication. Sample 1 utilizes the metals Ti, Pd, Cr, and Hf as metal contacts. In addition, to confirm the model consistency, we prepared a second sample incorporating only Ti and Au electrodes on a 5 mm long, 1.53 nm diameter semiconducting CNT. Optical images of samples are shown in Figure 1a and a magnified AFM image in Figure 1b. The metals Au, Ti, Pd, Cr, and Hf were chosen because they are nonferromagnetic and possess a wide range of work functions (4.0−5.2 eV).

## CHARACTERIZATION AND DISCUSSION

$I-V$ measurements were performed on the two samples in ambient environment

* Address correspondence to leeyoung@skku.edu, miy16@pitt.edu.

Received for review September 8, 2010 and accepted January 27, 2011.

**Published online February 10, 2011**
10.1021/nn102343k

© 2011 American Chemical Society

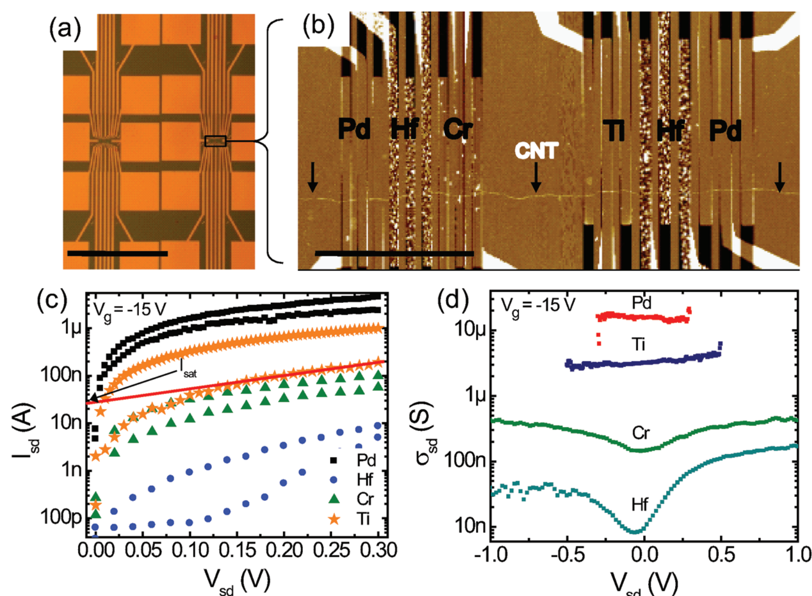


**Figure 1. Device structure and electrical properties of SWCNT. (a) Optical and (b) AFM images of CNTFET devices. Scale bar is 1 mm for optical and 20 $\mu$m for AFM image. (c) $I_{sd}$ vs $V_{sd}$ curves for a group of metals on the same CNT. Example of extrapolation procedure used to estimate $I_{sat}$ is shown in the case of a Ti contact. (d) Differential conductance curves for sample of Hf, Cr, Ti, and Pd metals exemplifying metal dependence.**

using a probe station. A back gate bias of $V_g = -15$ V was found to be sufficient to bias all devices in the hole-conducting on-state. This restriction was necessary to prevent the existence of multiple carrier types and eliminate the effect of threshold voltage shifts in the analysis of different metals. Figure 1c shows the clear $I_{sd}$ relationship with metals, with an order of $I$(Hf) < $I$(Cr) < $I$(Ti) < $I$(Pd). $I_{sat}$ is found by extrapolating the linear region of ln($I_{sd}$) vs $V_{sd}$ to $V_{sd} = 0$ V, as illustrated in Figure 1c. The corresponding $\sigma_{sd}$ curves are also provided in Figure 1d. To calculate $\sigma_{sd}$, $I_{sd}(V_{sd})$ curves were smoothed with a 16 point Savitzky Golay filter, and the resulting curves are differentiated. The data were tabulated by metal type, and differential conductance at $V_{sd} = 0$ point was chosen from each device for comparison.

To accurately compare $\sigma_{sd}$ and $I_{sat}$ for different metal contacts, statistical analysis is performed on the raw data to check the normality of each distribution. For data with a normal distribution, the mean will be used as an accurate comparative value to test for a dependence between metal $\sigma_{sd}$ and $I_{sat}$. Figure 2a shows a histogram of differential conductance by metal type. Although there is an overlap in the differential conductance for each metal, a distinct trend for $\sigma_{sd}$ is observed with an order, $\sigma_{sd}$(HF) < $\sigma_{sd}$(Cr) < $\sigma_{sd}$(Ti) < $\sigma_{sd}$(Pd). It will be demonstrated later in this report that the overlap is attributable to the widely varying and often overlapping work functions for each of the metal species. A Shapiro–Wilk normal distribution test of the data with $\alpha = 0.05$ permitted rejection of the normal distribution hypothesis for the metal Pd due to the wide asymmetric distribution of the data.[18] In this case, $\sigma_{sd}$ for Pd-contacted devices is very unlikely to be representative of a normal distribution, as expected due to the ohmic qualities of many devices limiting the upper range of conductance. To examine the dependence of mean $\sigma_{sd}$ on work function of Hf, Cr, Ti, and Au metal, ln($\sigma_{sd}$) *vs* work function (see Table S1, Supporting Information, for more details) is plotted in Figure 2b. A linear relationship between ln($\sigma_{sd}$) and work function is observed, although nonlinearity comes into play at large work function.

In order to understand the relationship between ln($\sigma_{sd}$) and work function, we begin with TFE current, since strict thermionic emission current and field emission current will give rise to a linear relationship. Pure thermionic emission theory also predicts that ln($\sigma_{sd}$)$\propto$ ($\Phi_{metal}$)/($kT$) = 38.61 (see data S1, Supporting Information). A simple linear fit of the data produces a slope <10, indicating the presence of a large field emission component. Therefore, a mixed TFE theory adopted from Crowell *et al.*[19] and Padovani *et al.*[20] is incorporated to fit the experimental observations. TFE current at a metal–semiconductor junction is described by

$$I_{sd} = I_{sat}[e^{V_{sd}/kT} - 1] \tag{1}$$

with

$$I_{sat} = \frac{A\pi^{1/2}{E_{00}}^{1/2}(\Phi_b - V_{sd} + \varsigma_2)^{1/2}}{kT\cosh\left(\frac{E_{00}}{kT}\right)} \times e^{\left(\frac{\varsigma_2}{kT} - \frac{\Phi_b + \varsigma_2}{E_0}\right)} \tag{2}$$

where $A$ is the Richardson constant, $T$ is temperature in Kelvin, $k$ is the Boltzmann constant, $\Phi_b$ is the Schottky barrier height, $\zeta_2 = E_F - E_V$, $E_F$ is the CNT Fermi level, $E_V$ is the CNT valence band, $E_{00}$ is a TFE tunneling parameter,[19] and $E_0 = E_{00}\coth(E_{00}/kT)$. Applying $V_g = -15$ V

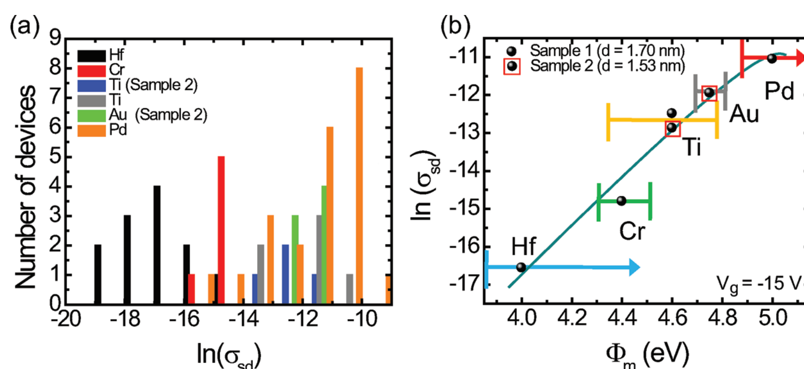


**Figure 2. Raw data of differential conductance ($\sigma_{sd}$) and fitting to theoretical thermionc field emission model. (a) Histograms of ln($\sigma_{sd}$) at $V_g = -15$ V. In order of smallest to largest mean value: Hf, Cr, Ti, Au, Pd; (b) ln($\sigma_{sd}$) plotted vs contact metal work function. The differential conductance value used for fitting each metal is the mean of the distributions in (a). Work function range is from the literature (T1, Supporting Information). Hf and Pd arrows are due to the possibility of large work function variations; in these cases the theoretical or only available literature values were chosen.**

results in $\zeta_2 = E_F - E_V \approx 0$, simplifying the system. We utilize the Schottky–Mott relationship and assume that $\Phi_b \approx \Phi_s - \Phi_m$. From the value of graphite, electron affinity, $X_{CNT} \approx 4.5$, and for a CNT diameter of 1.7 nm, energy gap, $E_g \approx 0.65$ eV.[21] Therefore, $\Phi_b \approx 5.15 - \Phi_m$, allowing replacement of the barrier dependence with a work function dependence. Further differentiating eq 1 and substituting eq 2 with the above relationships for $\Phi_b$, we derive (refer to data S2, Supporting Information for full derivation):

$$\ln(\sigma_{sd}) \propto \frac{1}{2}\ln(5.15 - \Phi_m) - \left(\frac{1}{E_0}\right)(5.15 - \Phi_m) \quad (3)$$

The fitting of this function to Hf, Cr, Ti, and Au is shown in Figure 2b. These results allow extraction of tunneling parameters $E_0 = 0.147$ eV $= E_{00}$ and $kT/E_{00} \approx 0.176$. The analysis of Crowell and Rideout is next used to find $\alpha_M = E_{carriers}/\Phi_b = \cosh(E_{00}/kT)^{-2}$,[19] where $\alpha_M$ is defined as a ratio of carrier energy $E_{carriers}$ to barrier height $\Phi_b$; $\alpha_M \approx 0$ from our model, indicating that most carriers tunnel directly to the valence band maximum. As a result of assumptions in the derivation, the excellent fit of eq 3 to the experimental observations strongly supports the existence of an unpinned Fermi level at metal–CNT interface. The source of the nonlinearity in Figure 2b results from growth of the logarithmic term in eq 3 as $\Phi_m \Rightarrow 5.15$. Phenomenologically, the energy barrier is sufficiently small and the field emission dominant such that variations in barrier height produce little to no change in differential conductance.

We next consider the saturation current of the above measured Schottky field effect transistors (SFETs) as a function of metal work function to further validate the theoretical model and the accurate fitting of the differential conductance. $I_{sat}$ for the metals was found by using both $\pm V_{sd}$ curves from all device measurements, as the positive and negative voltage regimes are correlated to the source/drain contacts separately (hence two $I_{sat}$ values for each device).[22] A histogram of the raw data is shown in Figure 3a. The Shapiro–Wilk normal distribution test of these data again allowed rejection of the possibility that Pd came from a normal distribution for $\alpha = 0.05$. The data set for the saturation current is significantly larger than that for differential conductance due to the use of both $\pm V_{sd}$ from raw data, hence (other than Pd) the distributions have more visually symmetrical shape.

Interestingly, the exact same TFE relationship as for $\sigma_{sd}$ can be used to fit $I_{sat}$, using equivalent work function and Fermi level assumptions (see data S3, Supporting Information). Pd was not included in the fitting, again because the sample mean was not reflective of the asymmetric distribution. Figure 3b shows ln($I_{sat}$) *vs* work function. The extracted tunneling parameters, $E_0 = 0.139 = E_{00}$ and $kT/E_{00} \approx 0.186$, are similar to those of differential conductance. This indicates that TFE and the derived model explain hole conduction in CNTFETs accurately.

Next, we consider the small variation of differential conductance (and $I_{sat}$) observed particularly in the case of Au and Cr in Figure 2. These metals are in contrast with Pd and Hf in which a large variation was observed. Further, if one fits the raw data variance onto the observed curve of ln($\sigma_{sd}$) *vs* $\Phi_b$, the resulting work function spread falls within the expected work function range observed in ambient, indicating strong correlation between local work function and $\sigma_{sd}$. This phenomenon is demonstrated in Figure S1, Supporting Information. It is therefore concluded that variation of $\sigma_{sd}$ (and $I_{sat}$) is strongly related to environmental stability of metal, since the work function can be easily modified by adsorbates (particularly in the case of Pd and Hf). Implication of our measurements and theoretical model fitting is very intriguing, particularly for gas sensing. Physisorption of gases on a metal alters the work function and surface dipole according to exposure dose, often by well-known relationships. While the metals display no change of conductance with exposure, when used as a contact to a CNT, the work

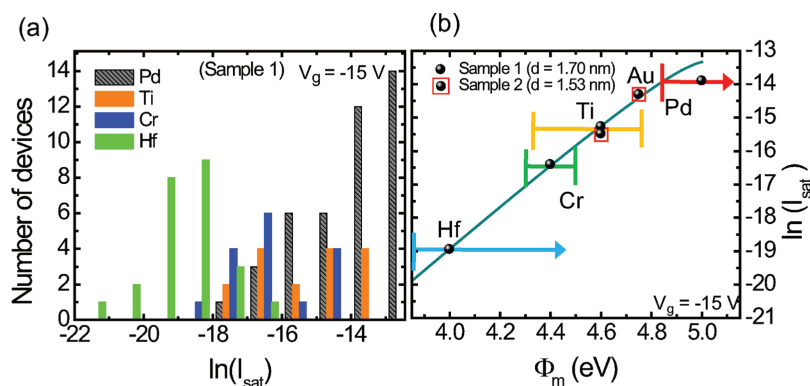


Figure 3. Raw data of ln($I_{sat}$) and fitting to theoretical thermionic field emission model. (a) Raw data of ln($I_{sat}$) at $V_g = -15$ as a function of metal. (b) Fitting of the mean values of ln($I_{sat}$) for Hf, Cr, and Ti to TFE model derived and discussed in the text. The error bounds for work function are taken from the literature (Table S1, Supporting Information). Hf and Pd arrows are due to possibility of large work function variations; in these cases the theoretical or only available literature values were chosen.

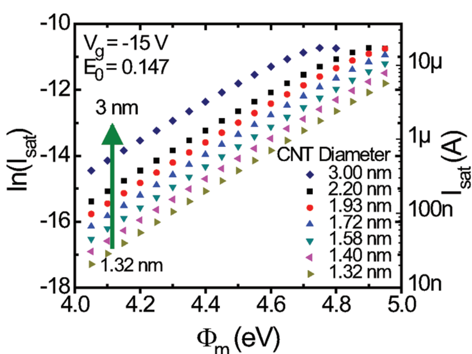


Figure 4. Simulation of diameter effect on ln($I_{sat}$) best fit curves. Simulated ln($I_{sat}$) curves for different diameter CNT using the model and constants from the text, assuming $E_{00} = 0.147$ and that all other factors except CNT work function are constant.

function and dipole change will result in a measurable $I_{sat}$ and $\sigma_{sd}$ difference explainable by the relationships derived in this report.

An initial constraint to this sensing approach is the variation in conducting properties for different CNT under varying initial environmental conditions. However, the use of different diameter CNT will only affect CNT work function, and a simulation of curves increased (decreased) saturation current for smaller (larger) diameter CNT is seen in Figure 4. Similar trends are visible for each diameter, but the model fails at a lower metal contact work function due to the smaller CNT work function in larger diameter tubes. In CNT with a diameter 3.0 nm, $I_{sat}$ approaches 15 $\mu$A, similar to what has been observed experimentally. This suggests that with large work function metal contacts, the model can also predict $I_{sat}$ in other CNT devices.[23] Therefore, simple $I-V$ measurement during exposure will allow extraction of the work function of the metal, which will in turn allow one to measure the existence and even the concentration of certain gas species, which previously has been impossible to quantify.

## CONCLUSION

In conclusion, we have demonstrated clear work function-dependent relationships for hole current $\sigma_{sd}$ and $I_{sat}$. These parameters have been correlated by an existing contact-dominant conduction mechanism. Using TFE theory, tunneling parameters were extracted using a novel characterization method that strongly suggests an unpinned Fermi level in carbon nanotubes. Additionally, the results for $\sigma_{sd}$ and $I_{sat}$ fittings are in agreement, and the mathematical model presented can also be utilized to selectivity sense adsorbates in single CNT sensors *via* contact work function change. The process could further be reversed to detect work function of a metal in the case of a well-controlled environment, an important discovery for materials where local probing or optical methods are impossible.

## METHODS

**Fabrication.** CNTs were synthesized by thermal CVD with $FeCl_3$ (Sigma Aldrich) in ethanol as a catalyst using flow rates of 16 sccm $H_2$, 8 sccm $CH_4$, and 100 sccm Ar in a 50 mm quartz tube. To contact the CNT with multiple metal species, modular Ti/Au probe-able pads were first fabricated with lead lines within ~15 $\mu$m of the CNT; *via* e-beam lithography (Raith eLine) and e-beam evaporation. Sequentially, Pd, Cr, Hf, and Ti electrodes were patterned with e-beam lithography, metal deposition performed by e-beam evaporation, and lift-off carried out in warm acetone. Post fabrication, CNTFET regions were covered with protective photoresist, and the samples were cleaned in 150 W $O_2$ plasma to remove unused CNTs.

**Characterization.** $I-V$ curves were measured using a Keithley 236 (Source/Drain) and Keithley 237 (Gate/Drain) with Labview interface. Data analysis was performed using plotting software Origin 8.0 (Origin Laboratories).

*Acknowledgment.* The Pittsburgh group would like to acknowledge the Air Force Office of Scientific Research through a

grant provided by MEST and NSF ECCS 1039543. The SKKU group would like to thank KICOS through a grant provided by MOST in 2007 (no. 2007-00202) and in part the Ministry of Education through the STAR-faculty project, TND Project, and the KOSEF through CNNC at SKKU.

*Supporting Information Available:* Derivation of limiting thermionic conditions and of eq 3 for $\sigma_{sd}$ and $I_{sat}$, correlation of data spread for $\sigma_{sd}$ and work function, and literature work functions. This information is available free of charge *via* the Internet at http://pubs.acs.org.

## REFERENCES AND NOTES

1. Heinze, S.; Tersoff, J.; Martel, R.; Derycke, V.; Appenzeller, J.; Avouris, P. Carbon Nanotubes as Schottky Barrier Transistors. *Phys. Rev. Lett.* **2002,** *89*, 106801.
2. Freitag, M.; Tsang, J. C.; Bol, A.; Yuan, D.; Liu, J.; Avouris, P. Imaging of the Schottky Barriers and Charge Depletion in Carbon Nanotube Transistors. *Nano Lett.* **2007,** *7*, 2037–2042.
3. Chen, Y. F.; Fuhrer, M. S. Tuning from Thermionic Emission to Ohmic Tunnel Contacts *via* Doping in Schottky-Barrier Nanotube Transistors. *Nano Lett.* **2006,** *6*, 2158–2162.
4. Leonard, F.; Tersoff, J. Role of Fermi-Level Pinning in Nanotube Schottky Diodes. *Phys. Rev. Lett.* **2000,** *84*, 4693.
5. Xue, Y.; Ratner, M. A. Schottky Barriers at Metal-Finite Semiconducting Carbon Nanotube Interfaces. *Appl. Phys. Lett.* **2003,** *83*, 2429–3.
6. Sze, S. M. *Physics of Semiconductor Devices*; Wiley-Interscience: New York, 1981.
7. Ding, L.; Wang, S.; Zhang, Z.; Zeng, Q.; Wang, Z.; Pei, T.; Yang, L.; Liang, X.; Shen, J.; Chen, Q.; *et al.* Y-Contacted High-Performance n-Type Single-Walled Carbon Nanotube Field-Effect Transistors: Scaling and Comparison with Sc-Contacted Devices. *Nano Lett.* **2009,** *9*, 4209–4214.
8. Shim, M.; Javey, A.; Kam, N. W. S.; Dai, H. Polymer Functionalization for Air-Stable n-Type Carbon Nanotube Field-Effect Transistors. *J. Am. Chem. Soc.* **2001,** *123*, 11512–11513.
9. Yu, W. J.; Kim, U. J.; Kang, B. R.; Lee, I. H.; Lee, E. H.; Lee, Y. H. Adaptive Logic Circuits with Doping-Free Ambipolar Carbon Nanotube Transistors. *Nano Lett.* **2009,** *9*, 1401–1405.
10. Zhang, Z.; Liang, X.; Wang, S.; Yao, K.; Hu, Y.; Zhu, Y.; Chen, Q.; Zhou, W.; Li, Y.; Yao, Y.; *et al.* Doping-Free Fabrication of Carbon Nanotube Based Ballistic CMOS Devices and Circuits. *Nano Lett.* **2007,** *7*, 3603–3607.
11. Chen, Z.; Appenzeller, J.; Lin, Y. M.; Sippel-Oakley, J.; Rinzler, A. G.; Tang, J.; Wind, S. J.; Solomon, P. M.; Avouris, P. An Integrated Logic Circuit Assembled on a Single Carbon Nanotube. *Science* **2006,** *311*, 1735.
12. Bachtold, A.; Hadley, P.; Nakanishi, T.; Dekker, C. Logic Circuits With Carbon Nanotube Transistors. *Science* **2001,** *294*, 1317–1320.
13. Chen, Z.; Appenzeller, J.; Knoch, J.; Lin, Y. M.; Avouris, P. The Role of Metal-Nanotube Contact in the Performance of Carbon Nanotube Field-Effect Transistors. *Nano Lett.* **2005,** *5*, 1497–1502.
14. Appenzeller, J.; Radosavljevic, M.; Knoch, J.; Avouris, P. Tunneling Versus Thermionic Emission in One-Dimensional Semiconductors. *Phys. Rev. Lett.* **2004,** *92*, 048301.
15. Nosho, Y.; Ohno, Y.; Kishimoto, S.; Mizutani, T. Relation Between Conduction Property and Work Function of Contact Metal in Carbon Nanotube Field-Effect Transistors. *Nanotechnology* **2006,** *17*, 3412–3415.
16. McClain, D.; Thomas, N.; Youkey, S.; Schaller, R.; Jiao, J.; O'Brien, K. P. Impact of Oxygen Adsorption on a Population of Mass Produced Carbon Nanotube Field Effect Transistors. *Carbon* **2009,** *47*, 1493–1500.
17. Yao, Y.; Li, Q.; Zhang, J.; Liu, R.; Jiao, L.; Zhu, Y. T.; Liu, Z. Temperature-Mediated Growth of Single-Walled Carbon-Nanotube Intramolecular Junctions. *Nat. Mater.* **2007,** *6*, 283–286.
18. Shapiro, S. S.; Wilk, M. B. An Analysis of Variance Test for Normality (Complete Samples). *Biometrika* **1965,** *52*, 591–611.
19. Crowell, C. R.; Rideout, V. L. Normalized Thermionic-Field (T-F) Emission in Metal-Semiconductor (Schottky) Barriers. *Solid-State Electron.* **1969,** *12*, 89–105.
20. Padovani, F. A.; Stratton, R. Field and Thermionic-Field Emission in Schottky Barriers. *Solid-State Electron.* **1966,** *9*, 695–707.
21. Weisman, R. B.; Bachilo, S. M. Dependence of Optical Transition Energies on Structure for Single-Walled Carbon Nanotubes in Aqueous Suspension: An Empirical Kataura Plot. *Nano Lett.* **2003,** *3*, 1235–1238.
22. Perello, D. J.; Lim, S. C.; Chae, S. J.; Lee, I.; Kim, M.; Lee, Y. H.; Yun, M. Current Anisotropy of Carbon Nanotube Diodes: Voltage and Work Function Dependence. *Appl. Phys. Lett.* **2010,** *96*, 263107–3.
23. Javey, A.; Guo, J.; Wang, Q.; Lundstrom, M.; Dai, H. J. Ballistic Carbon Nanotube Field-Effect Transistors. *Nature* **2003,** *424*, 654–657.